Mechanical and thermodynamic properties of cubic YH_2 under high pressure: Prediction from first-principles study*

Li Zhen-Li(李贞丽) and Cheng Xin-Lu(程新路)†

Institute of Atomic and Molecular Physics, Sichuan University, Chengdu 610064, *China*

(Received 28 July 2013; revised manuscript received 30 October 2013; published online 10 February 2014)

First-principles calculations are used to investigate the mechanical and thermodynamic properties of cubic YH_2 at different pressures and temperatures. The generalized gradient approximation (GGA) with Perdew–Burke–Ernzerhof (PBE) method is used to describe the exchange–correlation energy in the present work. The calculated equilibrium lattice constant a and bulk modulus B are in good accordance with the available experimental values. According to the Born–Huang criteria for mechanical stability, elastic constants are calculated from the strain-induced stress method in a pressure range from 0 to 67.1 GPa. Isotropic wave velocities and sound velocities are discussed in detail. It is found that the Debye temperature decreases monotonically with the increase of pressure and that YH_2 has low anisotropy in both longitudinal and shear-wave velocities. The calculated elastic anisotropic factors indicate that YH_2 has low anisotropy at zero pressure and that its elastic anisotropy increases as pressure increases. Through the quasi-harmonic Debye model, in which phononic effects are considered, the thermodynamic properties of YH_2, such as the relations of $(V–V_0)/V_0$ to the temperature and the pressure, the dependences of heat capacity C_v and thermal expansion coefficient α on temperature and pressure ranging from 0 to 2400 K and from 0 to 65 GPa, respectively, are also discussed.

Keywords: YH_2 density functional theory, mechanical properties, thermodynamic properties, quasi-harmonic Debye model

PACS: 62.20.de, 67.25.bd, 71.15.Mb **DOI:** 10.1088/1674-1056/23/4/046201

1. Introduction

Metal hydrides have been attracting attention for both fundamental and application researches for decades due to their important industrial applications. For example, metal hydrides are considered to be potential candidates for portable fuel cell applications because the hydrogen density in metal hydrides is larger than that in liquid hydrogen.[1,2] Granqvist *et al.*[3] and Huiberts *et al.*[4] pointed out the relevance of rare-earth (RE) hydrides for commercial energy saving windows, which can reduce the energy consumption of buildings. Yttrium hydride (YH_x), which is a metal hydride, is a very important material for ensuring the safety of the nuclear power systems because of advantages such as low-induced activity, low hydrogen desorption pressure, small neutron absorption cross section, high hydrogen density, phase stability, and cost reduction. Consequently, it is considered to be a good candidate for reflectors in fast breeder reactors.[5] In the 1970s, Beattie[6] measured the longitudinal and shear velocities of cubic polycrystalline $YH_{1.93}$. However, these data were limited between 80 K and 300 K. Vajda and Daou[7,8] described a study of YH_{2+x}, and observed the metal–semiconductor (MS) transition in a temperature range of 230 K–280 K for $x \sim 0.10$. By using the pseudopotential method, Wang and Chou[9] performed a systematic investigation of YH_{2+x} and found that the energy per H atom increases gradually as more and more excess hydrogen atoms (i.e., the value of x becomes bigger and bigger) are added. More recently, Kanagaprabha *et al.*[10] have analyzed the hydrogen storage capacity of Y–H system and found that the storage capacity increases as the number of hydrogen atoms increases, they also found the maximum storage capacity to be 3.28% in YH_3. Chihi *et al.*[11] carried out a study of the structure of YH_2 using the density functional theory and confirmed that YH_2 is mechanically stable.

It is universally received that the metal hydrides as potential hydrogen storage materials are susceptible to hydrogen embrittlement.[12] An understanding of the thermodynamics and stability of metal hydrides is, therefore, required to investigate and design potential hydrogen storage materials. In particular, the thermodynamic property of a material is key to its application in some modern technologies, in which the material is subjected to ultrahigh pressures and high temperatures. In this work, first-principles and quasi-harmonic Debye model[13] are employed to study the structure, elastic properties, isotropic wave velocities, heat capacity, and thermal expansion of YH_2 because some mechanical and thermodynamic properties of YH_2 must be studied and understood. The results obtained in our work may be useful for other groups working on this topic and may provide an important reference for the practical applications of YH_2.

*Project supported by the National Natural Science Foundation of China (Grant No. 11176020).

†Corresponding author. E-mail: chengxl@scu.edu.cn

© 2014 Chinese Physical Society and IOP Publishing Ltd

2. Method of calculation

The mechanical and thermodynamic properties of YH_2 at different pressures and temperatures were investigated by using the Cambridge Serial Total Energy Package (CASTEP) code[14,15] combined with the quasi-harmonic Debye model.[13] The generalized gradient approximation (GGA) with Perdew–Burke–Ernzerhof (PBE)[16] scheme was used to explore the electronic exchange and correlation energy. The plane-wave cutoff energy was 500 eV and Brillouin zone integration was carried out over the $10\times10\times10$ grid points using the Monkorst–Pack method[17] for the structure optimization. Y $4d^15s^2$ and H $1s^1$ were treated as valence electrons. The self-consistent convergence of the total energy was about 5.0×10^{-6} eV/atom and all forces on all of the atoms were converged to less than 0.01 eV/Å. The set of parameters assured a maximum atom displacement of 5.0×10^{-4} Å and a maximum stress of 0.02 GPa.

3. Results and discussion

3.1. Elastic properties

The CaF_2-type YH_2 has space group $Fm\bar{3}m$ (No. 255) with Y atom setting $4a$ (0, 0, 0) and H setting $8c$ (1/4, 1,4, 1/4). The equilibrium lattice constant a determined from a structural optimization is 5.286 Å. Using Birch–Murnaghan[18,19] fits for the total energy as a function of the lattice parameters, the bulk moduli B and its pressure derivative B' were obtained. These values, together with some theoretical and available experimental results, are given in Table 1. It is observed that our results are in good agreement with numerous experimental[5,7,20,21] and theoretical[10,11,22–24] data. It is indicated that the calculated method performed in our work is reasonable.

Table 1. Values of lattice constant a (Å), bulk modulus B (GPa), and the pressure derivative B' of YH_2 at zero pressure and zero temperature.

	Present work	Experiment	Other theoretical works
a/Å	5.286	5.203[a], 5.155[b], 5.208[c], 5.204[d]	5.298[e], 5.129[f], 5.200[g], 5.195[h], 5.204[i]
B/GPa	86.137	60.4[b], 86.44[c]	77.67[e], 108[f], 101.1[g], 84[h]
B'	3.646	10.08[b]	3.562[f], 5.5[h]
C_{11}/GPa	127.295		72.13[e], 230[f]
C_{12}/GPa	65.558		80.45[e], 48.3[f]
C_{44}/GPa	59.050		56.81[e], 90.8[f]

[a,b,c,d](Experiment) Refs. [7], [20], [5], [21]; [e](FP-GGA) Ref. [11]; [f](VASP) Ref. [10]; [g](FLAPW) Ref. [22]; [h](LDA) Ref. [23]; [i](KKR) Ref. [24]

A solid body changes its shape when being subjected to a stress. Provided that the stress is below the elastic limit, Hooke's law for a crystal is written as[25]

$$\sigma_{ij} = C_{ijkl}\varepsilon_{kl} \quad (i,j,k,l = 1,2,3), \tag{1}$$

where the fourth-rank tensor C_{ijkl} is the elastic stiffness tensor, σ_{ij} is the stress tensor, and ε_{kl} is the strain tensor. Thus, the elastic constants can be obtained directly from the calculation of the stress generated by forcing small strains to the optimized unit cell.[26,27] In general, there are 21 independent elastic constants C_{ij}, but this number of cubic crystals is reduced to only three when considering the symmetry of the crystal (C_{11}, C_{12}, C_{44}). The strained lattice vector $\boldsymbol{a}'$ used to determine the elastic constants is related to the unstrained lattice $\boldsymbol{a}$ by the relation

$$\boldsymbol{a}' = (\boldsymbol{I} + \varepsilon)\boldsymbol{a},$$

where $\boldsymbol{I}$ is the unit matrix. The strain tensor is

$$\varepsilon = \begin{pmatrix} e & e/2 & 0 \\ e/2 & 0 & 0 \\ 0 & 0 & 0 \end{pmatrix}. \tag{2}$$

So that Hooke's law gives

$$\sigma_{xx} = C_{11}e, \quad \sigma_{yy} = \sigma_{zz} = C_{12}e,$$
$$\sigma_{yz} = C_{44}e, \quad \sigma_{zx} = \sigma_{xy} = 0. \tag{3}$$

The ion positions are still fixed by the symmetry, so only electrons should be relaxed in the strained lattice. We first obtain the equilibrium primitive cell of YH_2 by optimizing the geometry and deformed the cell with the strain in equation (2) at a given pressure. Then, the strain-induced stresses discussed in the previous section are calculated and equation (3) is used to determine the values of C_{11}, C_{12}, and C_{44} for YH_2. The ratio of stress to strain versus strain is shown in Fig. 1(a). In this work, for all different strain magnitudes: $e = 0.02$, $e = 0.04$, $e = 0.06$, $e = 0.08$, $e = 0.10$ are used to deform the equilibrium primitive crystal, respectively. We repeat this procedure and calculate a series of values of C_{11}, C_{12}, and C_{44} at different pressures. As shown in Fig. 1(a), from the intercept of the best-fit line: $\sigma_{xx}/e = C_{11} + A(e)$, the values of C_{11}, C_{12}, and C_{44} are in successful agreement with the results calculated at zero pressure. The elastic constants completely specify the elastic properties and acoustic velocities of a single crystal.

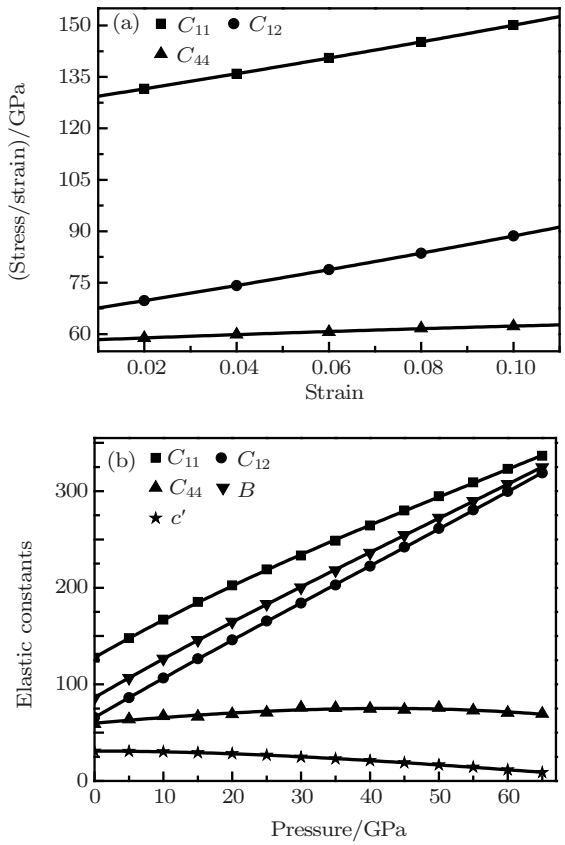


Fig. 1. (a) Stress/strain ratios versus strain. The solid lines represent linear fittings to the calculated values. (b) The elastic constants versus pressure at $T = 0$ K.

The elastic stiffness coefficients C_{ij} of solid are fundamental and indispensable for describing the connections between mechanical and dynamical behaviors of materials. These constants, which can give information about the stability and stiffness of a material, determine the response of the crystal to an external force. The elastic stiffness constants under hydrostatic pressure P, C_{ij}, are obtained by calculating the total energy as a function of volume conserving strain. The well-known Born–Huang criteria for the mechanical stability of cubic crystals are as follows:[28]

$$\tilde{C}_{\alpha\alpha} > 0, \quad \tilde{C}_{11} > \left|\tilde{C}_{12}\right|, \quad \tilde{C}_{11} + 2\tilde{C}_{12} > 0, \tag{4}$$

where

$$\tilde{C}_{\alpha\alpha} = C_{\alpha\alpha} - P, \ (\alpha = 1, 4),$$

and $\tilde{C}_{12} = C_{12} + P$.

As for hydrostatic pressure P, the bulk modulus B and shear modulus G are related to the elastic stiffness constants C_{ij} by the following relations:[29,30]

$$G = (G_{\mathrm{V}} + G_{\mathrm{R}})/2, \tag{5}$$

$$B = (C_{11} + 2C_{12})/3, \tag{6}$$

$$G_{\mathrm{V}} = \frac{2c'}{5} + \frac{3C_{44}}{5}, \tag{7}$$

$$G_{\mathrm{R}} = \frac{10c'C_{44}}{6c' + 4C_{44}}, \tag{8}$$

where

$$c' = (C_{11} - C_{12})/2,$$

G_{V} and G_{R} are the averaged polycrystalline shear moduli according to the Voigt and Reuss shear modulus. The calculated results show that, when the pressure is less than 67.1 GPa, the elastic constants of YH_2 satisfy equation (4), indicating that the crystal structure of YH_2 is still fcc. Consequently, we investigate the elastic properties of YH_2 under high pressures ranging from 0 to 67.1 GPa.

The variations of elastic stiffness constants C_{ij} and bulk modulus B are plotted in Fig. 1(b). It is noted that C_{11}, C_{12}, and C_{44} increase linearly with the increase of pressure, while the varying amplitude of C_{44} is most moderate with respect to C_{11} and C_{12}. The change in c' is inversely proportional to pressure, and the amplitude of variation is obvious. The elastic constant C_{11} corresponds to elasticity in length, and the elastic constants C_{12} and C_{44} are related to elasticity in shape. This variation of C_{11} indicates that pressure will produce obvious change lengthwise and that the small C_{44} means a low ability to resist the shear distortion in the (100) plane. The elastic compliance constants S_{ij} have also been calculated from C_{ij} and tabulated below. The compressibility coefficient K and Poisson's ratio ν are two important factors for technological and engineering applications. It is universally received that bulk modulus or shear modulus is associated with hardness, and the compressibility coefficient K can measure the hardness indirectly. Our calculated results at different pressures summarized in Table 2 demonstrate that YH_2 is a highly compressible material. Additionally, a high (low) B/G value suggests the ductility (brittleness) of a material and that the critical value which separates ductile and brittle materials is approximately 1.75.[31] Our calculated ratio B/G of YH_2 is 1.89, which means that YH_2 belongs to ductile material. According to the Frantsevich rule,[32] the Poisson's ratio ν can distinguish the ductility and brittleness of materials. The critical value that separates ductile and brittle materials is 0.33.[32] If $\nu > 0.33$, the material behaves in a ductile manner; otherwise the material is expected to be brittle. Here, the calculated values of ν are larger than 0.33, which highlights the ductile nature of YH_2. The compressibility coefficient K and Poisson's ratio ν are defined by the following expression:[33]

$$K = \frac{1}{B} = \frac{3}{(C_{11} + 2C_{12})}, \tag{9}$$

$$\nu = \frac{C_{12}}{(C_{11} + C_{12})}. \tag{10}$$

Table 2. Values of lattice constant (Å), density (g/cm^3), elastic compliances (10^{-2} GPa^{-1}), elastic moduli (GPa), compressibility coefficient K (10^{-3} GPa^{-1}), Possion's ratio v, wave velocities (km/s), and Debye temperature (K) for YH_2 from 0 to 67.1 GPa.

P/GPa	a/Å	ρ/g·cm^{-3}	$S_{11}/10^{-2}$ GPa^{-1}	$S_{12}/10^{-2}$ GPa^{-1}	$S_{44}/10^{-2}$ GPa^{-1}	B/GPa	G_V/GPa	G_R/GPa	G/GPa	c'/GPa	$K/10^{-3}$ GPa	v	V_P/km·s^{-1}	V_S/km·s^{-1}	θ_D/K
0	5.286	4.088	1.21	–0.41	1.69	86.1	47.8	43.3	45.5	30.9	11.61	0.340	6.00	3.34	479.1
5	5.196	4.305	1.19	–0.44	1.57	106.7	50.6	44.7	47.7	30.8	9.37	0.368	6.29	3.33	487.9
10	5.122	4.494	1.19	–0.46	1.49	126.5	52.4	45.1	48.8	30.2	7.90	0.389	6.53	3.29	491.6
15	5.060	4.622	1.21	–0.49	1.50	146.0	51.7	44.2	47.9	29.4	6.85	0.406	6.71	3.21	485.8
20	5.006	4.814	1.25	–0.52	1.45	164.8	52.8	43.7	48.2	28.2	6.07	0.419	6.90	3.17	485.7
25	4.958	4.955	1.31	–0.56	1.41	183.2	53.2	42.7	48.0	26.8	5.46	0.430	7.06	3.11	482.8
30	4.916	5.083	1.41	–0.62	1.32	200.4	55.4	41.4	48.4	24.6	4.99	0.441	7.22	3.09	483.7
35	4.877	5.206	1.51	–0.68	1.32	218.0	54.5	39.4	46.9	22.9	4.59	0.449	7.34	3.00	475.0
40	4.841	5.322	1.63	–0.74	1.34	236.3	53.2	37.0	45.1	21.1	4.23	0.457	7.46	2.91	464.7
45	4.809	5.432	1.80	–0.83	1.36	254.6	51.8	34.3	43.0	19.0	3.93	0.464	7.58	2.81	452.9
50	4.778	5.536	2.04	–0.96	1.32	272.4	52.1	31.4	41.7	16.7	3.67	0.470	7.70	2.75	445.0
55	4.750	5.635	2.37	–1.13	1.37	289.9	49.5	27.6	38.5	14.3	3.45	0.476	7.78	2.61	426.9
60	4.723	5.731	2.91	–1.40	1.42	307.3	47.0	23.3	35.1	11.6	3.25	0.481	7.86	2.48	406.8
65	4.699	5.822	3.80	–1.85	1.44	324.6	45.3	18.6	32.0	8.9	3.08	0.486	7.94	2.34	387.5
67	4.689	5.858	4.35	–2.12	1.48	331.5	43.5	16.5	30.0	7.7	3.02	0.488	7.96	2.26	375.1
67.1	4.689	5.860	4.38	–2.14	1.50	331.8	43.1	16.4	29.7	7.7	3.01	0.489	7.96	2.25	373.5

3.2. Isotropic wave velocities

The Debye temperature, as an important fundamental parameter, is closely related to many physical properties of solids, such as elastic constants, melting temperature, and specific heat. One can calculate the Debye temperature Θ_D from elastic constant data, since Θ_D is proportional to the averaged sound velocity V_m, via the following equation[34]

$$\Theta_D = \frac{h}{k}\left[\frac{3n}{4\pi}\left(\frac{N_A\rho}{M}\right)\right]^{1/3} V_m, \tag{11}$$

where h is the Planck's constant, k the Boltzmann's constant, N_A the Avogadro's number, n the number of atoms in the molecule, M the molecular weight and ρ the density. The averaged sound velocity can be computed from[35]

$$V_m = \left[\frac{1}{3}\left(\frac{2}{V_S^3}+\frac{1}{V_P^3}\right)\right]^{-1/3}, \tag{12}$$

where V_P and V_S are the longitudinal and shear-wave velocities, respectively, which can be calculated for both cubic and hexagonal crystals, are obtained from Navier's equation as[36]

$$V_P = \sqrt{\frac{B+4G/3}{\rho}} \quad \text{and} \quad V_S = \sqrt{\frac{G}{\rho}}. \tag{13}$$

Figure 2 shows the predicted pressure dependences of the longitudinal wave velocity, shear-wave velocity, and average velocity, V_P, V_S, and V_m. The longitudinal wave velocity increases with an increase of pressure, while the shear-wave velocity decreases with an increase of pressure. At 0 K, using the present elastic constants, we obtain $\Theta_D = 479.1$ as listed in Table 2.

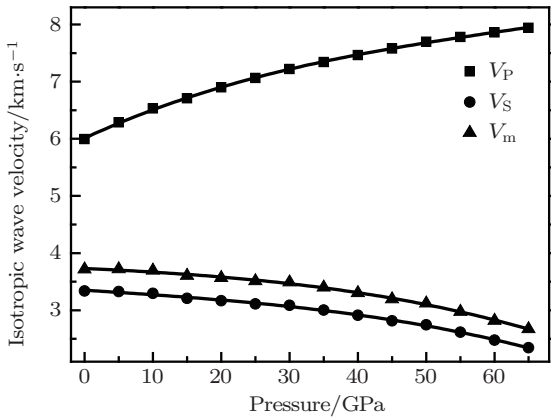


Fig. 2. Values of longitudinal wave V_P, shear-wave V_S, and average velocities V_m versus pressure P.

3.3. Sound velocities

The acoustic vibrational modes of a solid in the long wavelength limit are obtained from the Christoffel equation,[37]

$$\rho\omega^2 u_i = M_{il}u_l, \tag{14}$$

where ρ is the mass density, ω the vibrational angular frequency, u_i the displacement amplitudes, and summation convention is used for repeated Cartesian indices. The matrix M_{il} is given by

$$M_{il} = c_{ijkl}k_j k_k, \tag{15}$$

where c_{ijkl} is the elastic constant tensor elements, and k_j the wave vector components of the vibrational wave. Using Voigt notation, in the case of a cubic crystal, the M_{il} matrix reduces to

$$\begin{pmatrix} C_{11}k_x^2+(k_y^2+k_z^2)C_{44} & (C_{12}+C_{44})k_xk_y & (C_{12}+C_{44})k_xk_z \\ (C_{12}+C_{44})k_xk_y & C_{11}k_y^2+(k_x^2+k_z^2)C_{44} & (C_{12}+C_{44})k_yk_z \\ (C_{12}+C_{44})k_xk_z & (C_{12}+C_{44})k_yk_z & C_{11}k_z^2+(k_x^2+k_y^2)C_{44} \end{pmatrix}. \tag{16}$$

For any direction, the eigenvectors will be a quadratic function of $k = |\boldsymbol{k}|$ and hence $\omega = V_n(\hat{k})k$ with $V_n(\hat{k})$ being the sound velocity for polarization n and direction $\hat{k}$. For example, for $\boldsymbol{k}$ along [100], $k_y = k_z = 0$ and $k_x = 1$, the sound velocities become

$$V_{\mathrm{LA}}([100]) = \sqrt{C_{11}/\rho}, \tag{17}$$

$$V_{\mathrm{TA1}}([100]) = V_{TA2}([100]) = \sqrt{C_{44}/\rho}, \tag{18}$$

where V_{LA} denotes longitudinal velocity; and V_{TA1} and V_{TA2} denote the shear-wave velocities polarized in the $(\bar{1}10)$ plane (s_1) and (001) plane (s_2) along the propagation direction [100], respectively.

Similarly, for the [110] wave vector direction, the sound velocities are defined by the results:

$$V_{\mathrm{LA}}([110]) = \sqrt{\frac{1}{2}\left(C_{11}+C_{12}+2C_{44}\right)/\rho}, \tag{19}$$

$$V_{\mathrm{TA1}}([110]) = \sqrt{\frac{1}{2}\left(C_{11}-C_{12}\right)/\rho}, \tag{20}$$

$$V_{\mathrm{TA2}}([110]) = \sqrt{C_{44}/\rho}. \tag{21}$$

And for the [111] wave vector direction:

$$V_{\mathrm{LA}}([111]) = \sqrt{\frac{1}{3}\left(C_{11}+2C_{12}+4C_{44}\right)/\rho}, \tag{22}$$

$$V_{\mathrm{TA1}}([111]) = V_{\mathrm{TA2}}([111])\sqrt{\frac{1}{3}\left(C_{11}-C_{12}+C_{44}\right)/\rho}. \tag{23}$$

For the face-centred cubic structure YH_2, the anisotropies of the wave polarized in the direction perpendicular to the basal plane (s_1) and the one polarized in the basal plane (s_2) have the anisotropies[38]

$$\Delta s_1 = \frac{1}{\Delta s_2} = \frac{C_{11}-C_{12}}{2C_{44}} = \frac{c'}{C_{44}}. \tag{24}$$

It is required by equation (24) that Δs_1 must be unity for isotropic crystals. The pressure dependences of Δs_1 at pressures up to 65 GPa are shown in Fig. 5. It is seen that Δs_1 descends with the increase of pressure, which is attributed to the fact that c' is greatly affected by pressure.

Figure 3 shows the pressure dependences of the sound velocities, the lines are the third-order polynomial fitting to the results. It is found that YH_2 has low anisotropy in both longitudinal and shear-wave velocities. Both the longitudinal velocities along the directions [110] and [111] monotonically increase with the increase of pressure, starting from zero pressure, while the shear-wave velocities along the directions [110] and [111] move slightly downward instead of upward. However, the behaviors of sound velocities for the [100] propagation direction are just the reverse scenario.

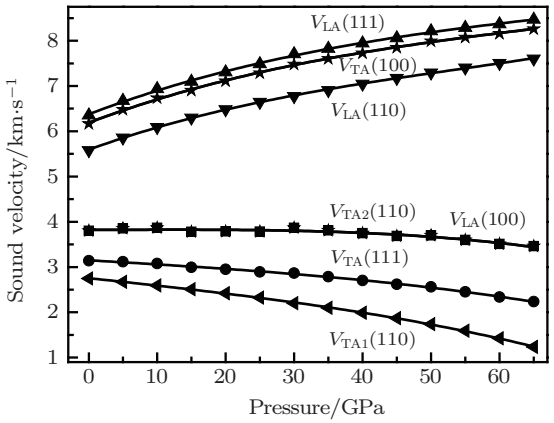


Fig. 3. Calculated pressure dependences of the sound velocities in YH_2.

3.4. Elastic anisotropy factor

As is well known, a superhard material must preferably be isotropic, otherwise it would deform preferentially in a given direction.[39] In other words, microcracks are easily induced in the material due to the significant elastic anisotropy.[40] Hence, it is important to calculate elastic anisotropy in order to predict new hard materials and improve their mechanical durability values. The elastic anisotropy of a crystal is the orientation dependences of the elastic moduli or sound velocities. A proper description of an anisotropy behavior has important implications in engineering science as well as in crystal physics.[41] For cubic crystals, the elastic anisotropy factor is expressed as

$$A = \frac{2C_{44}}{C_{11}-C_{12}} = \Delta s_2, \tag{25}$$

which is unity for an isotropic crystal and any value of A either smaller or greater than unity corresponds to the degree of elastic anisotropy possessed by the crystal. For an isotropic crystal, G_{V} given by equation (7) and G_{R} given by equation (8) from the Voigt and Reuss assumptions represent the theoretical maximum and minimum limits of the true shear modulus for the isotropic polycrystalline aggregate, respectively.[42] In the following, we extract the two limiting shear moduli G_{V} and G_{R} and take the difference between them as a measure of the elastic anisotropy. This difference in terms of C_{ij} is[42]

$$G_{\mathrm{V}} - G_{\mathrm{R}} = \frac{3}{5}\frac{\left(2c'-2C_{44}\right)^2}{6c'+4C_{44}}. \tag{26}$$

It is noted that the numerator is zero for isotropic materials; namely, $G_{\mathrm{V}} = G_{\mathrm{R}}$. For highly anisotropic crystals, however, the difference $(G_{\mathrm{V}} - G_{\mathrm{R}})$ would be considerably proportional to the magnitude of the elastic anisotropy possessed by the crystal.

Then, a new dimensionless quantity A^* is introduced such that[42]

$$A^* = (G_{\mathrm{V}} - G_{\mathrm{R}})/(G_{\mathrm{V}} + G_{\mathrm{R}}), \tag{27}$$

or in terms of C_{ij}, A^* is transformed as follows:

$$A^* = \frac{3\left(2c' - 2C_{44}\right)^2}{12c'^2 + 76c'C_{44} + 12C_{44}^2}. \tag{28}$$

Dividing each term of both denominator and numerator by c'^2 and rearranging the result, equation (28) turns into

$$A^* = \frac{3\left(A-1\right)^2}{3\left(A-1\right)^2 + 25A}. \tag{29}$$

Equation (29) is an important result of the present analysis and it describes the degree of elastic anisotropy for cubic crystal. We can know that A^* is always positive and a single-valued measure of the elastic anisotropy presented in crystal. Furthermore, A^* (in percent) just gives the relative magnitude of the elastic anisotropy presented in crystal. In our work, we find the elastic anisotropy specified by equation (29) is 4.94% for YH_2 at zero pressure, and the degree of anisotropy increases with rising pressure, as shown in Fig. 4. Taking the crystal of NbN with rock-salt structure as an example, its elastic anisotropy calculated from the elastic constants (at 0 GPa) is 16.87%;[43], thus one may conclude form this that YH_2 exhibits lower anisotropy than NbN. This conclusion is in accordance with the actual data on the orientation-dependent shear moduli in these crystals.

The use of a normalized elastic constant C'_{ij} that enables us to investigate elasticity in more detail is another way to estimate elastic anisotropy. The C'_{ij} is defined by dividing a specific elastic constant with the bulk modulus as[44]

$$C'_{ij} = \frac{C_{ij}}{B} = \frac{3C_{ij}}{(C_{11} + 2C_{12})}. \tag{30}$$

In an elastically ideal cubic crystal (the isotropic Cauchy solid), the conditions $C'_{11} = 1.8$, $C'_{12} = 0.6$, $C'_{44} = 0.6$ are satisfied at zero pressure.[44] We find that our values of C'_{11}, C'_{12}, and C'_{44} are 1.48, 0.76, and 0.69, respectively, which slightly deviates from the ideal values. These small deviations clearly highlight low elastic anisotropy.

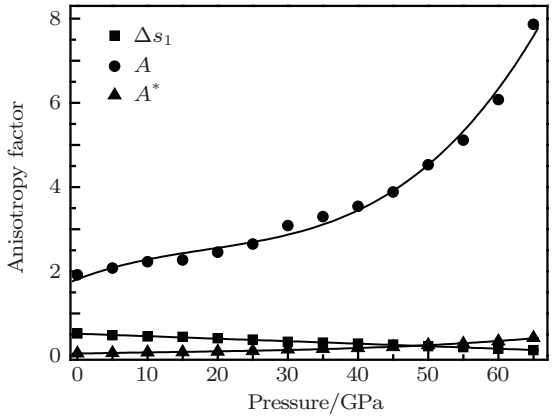


Fig. 4. Anisotropy factors, Δs_1, A, and A^* versus pressure for YH_2 in a range of 0 GPa–65 GPa.

3.5. Thermodynamic properties

In order to investigate the thermodynamic properties of YH_2, we employ the quasi-harmonic Debye model,[13] in which the non-equilibrium Gibbs function $G^*(V;P,T)$ can be written as follows:

$$G^*(V;P,T) = E(V) + PV + A_{\rm vib}(\Theta(V);T), \tag{31}$$

where $E(V)$ is the total energy per unit cell, P is the constant hydrostatic pressure condition, $\Theta(V)$ is the Debye temperature, and $A_{\rm vib}$ is the vibrational Helmholtz free energy, which can be written using the quasi-harmonic approximation[11] and Debye model of phonon density of states as[13,45–47]

$$A_{\rm vib}(\Theta;T) = nKT\left[\frac{9}{8}\frac{\Theta}{T} + 3\ln\left(1 - {\rm e}^{-\Theta/T}\right) - D\left(\frac{\Theta}{T}\right)\right], \tag{32}$$

where n is the number of atoms per formula unit, $D(\Theta/T)$ is the Debye integral. And, for an isotropic solid, Θ can be taken as[46]

$$\Theta = \frac{\hbar}{K}\left[6\pi^2 V^{1/2} n\right]^{1/3} f(\sigma)\sqrt{\frac{B_{\rm S}}{M}}, \tag{33}$$

where M is the molecular mass per unit cell, $f(\sigma)$ is given in Refs. [48] and [49], Poisson σ is taken to be 0.25,[50] $B_{\rm S}$ denotes the adiabatic bulk modulus, which is approximated by the static compressibility and expressed by[13]

$$B_{\rm S} \approx B(V) = V\left(\frac{{\rm d}^2 E(V)}{{\rm d}V^2}\right). \tag{34}$$

Therefore, the non-equilibrium Gibbs function $G^*(V;P,T)$ as a function of V, P, and T can be minimized with respect to volume V by taking

$$\left[\frac{\partial G^*(V;P,T)}{\partial V}\right]_{P,T} = 0. \tag{35}$$

The heat capacity C_v and the thermal expansion coefficient α are given by[51]

$$C_v = 3nk\left[4D\left(\frac{\Theta}{T}\right) - \frac{3\Theta/T}{{\rm e}^{(\Theta/T)} - 1}\right], \tag{36}$$

$$\alpha = \frac{\gamma C_V}{B_T V}, \tag{37}$$

where γ is the Grüneisen parameter, which is defined as

$$\gamma = -\frac{{\rm d}\ln\Theta(V)}{{\rm d}\ln V}. \tag{38}$$

Using the above methods, the thermodynamic properties of various substances have been successfully predicted.[52–55] In our work, the thermodynamic properties of a YH_2 are determined in a temperature from 0 K to 2400 K, where the quasi-harmonic model remains fully valid. The pressure effect is investigated in a pressure range from 0 GPa to 65 GPa. Figure 5(a) shows the variations of $(V–V_0)/V_0$ with pressure at

different temperatures, and figure 5(b) displays the relationships between $(V–V_0)/V_0$ and temperature at different pressures, where V_0 is the cell volume at $P = 0$ and $T = 0$. It is clearly seen that, when $(V–V_0)/V_0 > 0$, the cell volume is expanded, while $(V–V_0)/V_0 < 0$ indicates that the cell is compressed. The absolute value of $(V–V_0)/V_0$ is the volume variation of the crystal cell volume. As is well known, temperature can expand a cell and pressure can suppress this effect; in other words, the effects of temperature and pressure on the cell are opposite. From Fig. 5, we can see that $(V–V_0)/V_0$ decreases with the increase of pressure, and increases with the rise of temperature at zero pressure. While at a given pressure, a higher temperature will make the cell expansion easier. When the temperature is 2400 K, just 3.91 GPa of pressure can restrain the volume expansion caused by temperature: cell volume is still V_0, which suggests that the volume variation is more sensitive to pressure. Figure 5(b) shows that the crystal lattice expands evidently at high temperature with low pressure. However, the expanding effect is suppressed and the variation is restrained as the pressure increases. That is to say, the thermal effect is suppressed at high pressure. The result is consistent with that in Fig. 5(a).

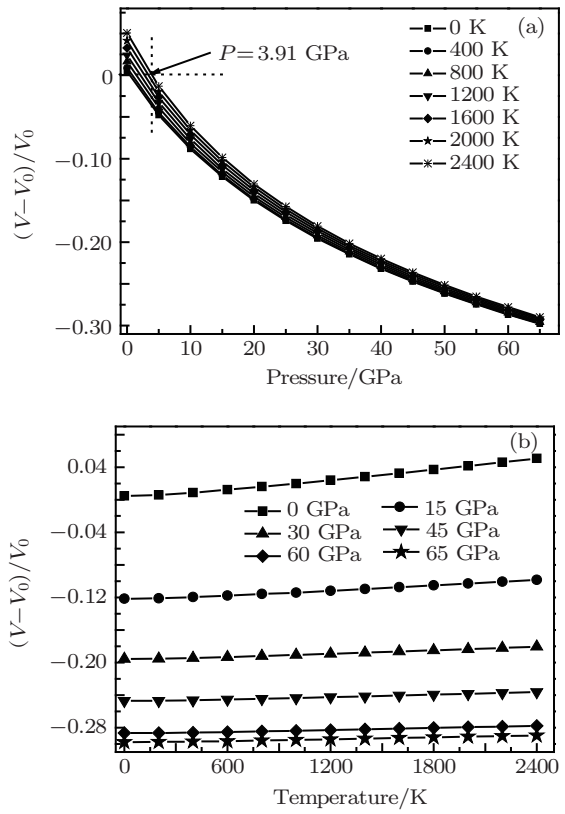


Fig. 5. Variations of $(V–V_0)/V_0$ with pressure P at different temperatures (a) and temperature T at different pressures P (b), where V_0 is the cell volume at $P = 0$ and $T = 0$.

The variations of heat capacity and thermal expansion with temperature at different pressures are depicted in Fig. 6. The relevant investigation on heat capacity of crystals is an old topic of condensed matter physics. Knowledge of the heat capacity of a substance not only provides an essential insight into the vibrational properties, but also possesses many applications. Two well-known limiting cases are correctly predicted by the standard elastic continuum theory.[56] At high temperatures, the constant-volume heat capacity C_v tends to the Petit and Dulong limit.[57] At sufficiently low temperatures, C_v is proportional to T^3.[57] At intermediate temperatures, however, the temperature dependence of C_v is governed by the details of vibrations of the atoms. In Fig. 6(a), C_v increases as temperature increases at a given pressure, and decreases as pressure rises at a given temperature. It is noted that, when $T < 400$ K, C_v increases sharply with rising temperature, which is due to the harmonic approximation of the Debye model. However, when temperature goes up to 400 K, the increase gradually slows down and C_v tends to the Dulong–Petit limit (≈ 74.65 J·mol^{-1}·K^{-1}), which is common to all solids at high temperatures.

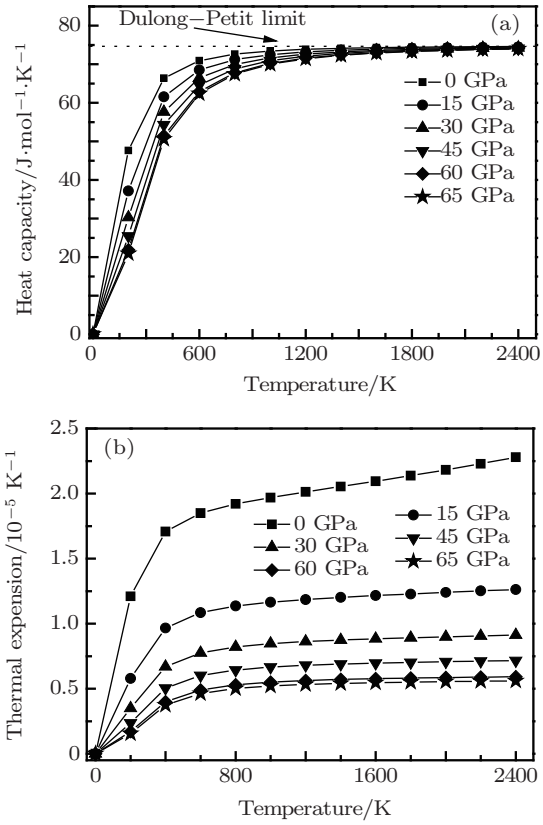


Fig. 6. (a) Plots of heat capacity versus temperature at different pressures. (b) Plots of thermal expansion versus temperature at pressures in a range of 0–65 GPa.

The curves of thermal expansion coefficient α–T are plotted in Fig. 6(b), showing that when temperature T is below 400 K, α rises rapidly with the increase of temperature, especially at zero or low pressure, and then the ascending tendency becomes weaker at high temperatures. At a certain temperature, the thermal expansion α decreases with the increase of pressure, and α under higher pressure is smaller, which is absolutely consistent with the scenario in Fig. 6(b). Moreover,

when the pressure $P = 65$ GPa, $T > 600$ K, α hardly changes any more, which means that under high pressure the effects of temperature on the thermal expansion of YH_2 are suppressed. Finally, we predict that the expansion coefficient α of fcc YH_2 is approximate to 1.71×10^{-5} K^{-1} at 400 K and 0 GPa.

4. Conclusions

In this paper we have investigated the mechanical and thermodynamic properties at different pressures and temperatures by plane-wave pseudopotential density functional theory (DFT) and the quasi-harmonic Debye model. The equilibrium lattice parameters are consistent with a few available experimental values and other theoretical data. According to Born–Huang criteria for mechanical stability, it is found that the crystal structure of YH_2 is stable at pressures less than 67.1 GPa, and the elastic constants calculated from strain-induced stresses method at pressures ranging from 0 GPa to 67.1 GPa are presented. The compressibility coefficient K and ratio B/G of YH_2 are 11.61×10^{-3} GPa^{-1} and 1.89 at 0 GPa, respectively, which indicates that YH_2 is a potentially compressible and ductile material. The pressure dependences of isotropic wave velocities and sound velocities are also discussed. The Debye temperature decreases monotonically with the increase of pressure, and YH_2 has low anisotropy in both longitudinal and shear-wave velocities. The low dimensionless quantity A^* and small deviations from the ideal values of normalized elastic constants C'_{ij} at zero pressure suggest the low elastic anisotropy of YH_2. In addition, we carry out a study of the thermodynamic properties by the quasi-harmonic Debye model. The heat capacity C_v is proportional to T^3 at sufficiently low temperatures, and it is close to the Dulong–Petit limit (≈ 74.65 $J\cdot mol^{-1}\cdot K^{-1}$) at high temperatures. Furthermore, the thermal expansion α rises as temperature increases, and the ascending trend becomes weaker at high temperatures. We predict that the thermal expansion coefficient α of YH_2 is 1.71×10^{-5} K^{-1} at 0 GPa and ambient temperature.

References

[1] Viswall R and Alefeld G 1978 *Hydrogen Storage in Metals II* (Berlin: Springer) p. 201
[2] Latroche M J 2004 *Phys. Chem. Solids* **65** 517
[3] Granqvist C G, Azens A, Hjelm A, Kullman L, Niklasson G A, Rönnow D, Strømme Mattsson M, Veszelei M and Vaivars G 1998 *Solar Energy* **63** 199
[4] Huiberts J N, Griessen R, Rector J H, Wijngaarden R J, Dekker J P, de Groot D G and Koeman N J 1996 *Nature* **380** 231
[5] Ito M, Setoyama D, Matsunaga J, Muta H, Kurosaki K, Uno M and Yamanaka S 2006 *J. Alloys Compd.* **426** 67
[6] Beattie A G 1972 *J. Appl. Phys.* **43** 3219
[7] Vajda P and Daou J N 1991 *Phys. Rev. Lett.* **66** 3176
[8] Daou J N and Vajda P 1992 *Phys. Rev. B* **45** 10907
[9] Wang Y and Chou M Y 1993 *Phys. Rev. B* **49** 10731
[10] Kanagaprabha S, Asvinimeenaatci A T, Sudhapriyanga G, Jemmy Cinthia A, Rajeswarapalanichamy R and Iyakutti K 2013 *Acta Phys. Pol. A* **123** 126
[11] Chihi T, Fatmi M and Bouhemadou A 2012 *Solid State Sci.* **14** 583
[12] Vehoff H 1997 in: *Hydrogen in Metals III, Properties and Applications*, ed. Wipf H (Berlin: Springer-Verlag) p. 215
[13] Blanco M A, Francisco E and Luaña V 2004 *Comput. Phys. Commun.* **158** 57
[14] Segall M D, Lindan P J D, Probert M J, Pickard C J, Hasnip P J, Clark S J and Payne M C 2002 *J. Phys.: Condens. Matter* **14** 2717
[15] Milman V, Winkler B, White J A, Pickard C J, Payne M C, Akhmatskaya E V and Nobes R H 2000 *Int. J. Quantum Chem.* **77** 895
[16] Perdew J P, Burke K and Ernzerhof M 1996 *Phys. Rev. Lett.* **77** 3865
[17] Pack J D and Monkhorst H J 1977 *Phys. Rev. B* **16** 1748
[18] Murnaghan F D 1944 *Proc. Natl. Acad. Sci. USA* **30** 244
[19] Birch F 1986 *J. Geophys. Res.* **91** 4949
[20] Machida A, Ohmura A, Watanuki T, Ikeda T, Aoki K, Nakano S and Takemura K 2006 *Solid State Commun.* **138** 436
[21] Pebler A and Wallace W E 1962 *J. Phys. Chem.* **66** 148
[22] Wolf W and Herzig P 2000 *J. Phys.: Condens. Matter* **12** 4535
[23] Sun S N, Wang Y and Chou M Y 1994 *Phys. Rev. B* **49** 6481
[24] Peterman D J, Harmon B N and Marchiando J 1979 *Phys. Rev. B* **19** 4867
[25] Nye J F 1985 *Physical Properties of Crystals* (Oxford: Clarendon) p. 329
[26] Wentzcovitch R M, Ross N L and Price G D 1995 *Phys. Earth Planet. Interiors* **90** 101
[27] Karki B B, Stixrude L, Clark S J, Warren M C, Ackland G J and Crain J 1997 *Am. Mineral.* **82** 51
[28] Sin'ko G V and Smirnow N A 2002 *J. Phys.: Condens. Matter* **14** 6989
[29] Zha C S, Mao H K and Hemley R J 2000 *Proc. Natl. Acad. Sci. USA* **97** 13494
[30] Wang J H, Li J, Yip S, Phillpot S and Wolf D 1995 *Phys. Rev. B* **52** 12627
[31] Pugh S F 1954 *Philos. Mag.* **45** 823
[32] Frantsevich I N, Voronov F F and Bokuta S A 1983 *Elastic Constants and Elastic Moduli of Metals and Insulators Handbook* (Kiev: Naukuva Dumka) pp. 60–180
[33] Wdowik U D, Parliński K and Siegel A 2006 *J. Phys. Chem. Solids* **67** 1477
[34] Anderson O L 1963 *J. Phys. Chem. Solids* **24** 909
[35] Lu L Y, Cheng Y, Chen X R and Zhu J 2005 *Physica B* **370** 236
[36] Schreiber E, Anderson O L and Soga N 1973 *Elastic Constants and Their Measurements* (New York: McGrawHill)
[37] Landau L D and Lifschitz E M 1980 *Theory of Elasticity, Course of Theoretical Physics* (New York: Pergamon Press)
[38] Wang H Y, Chen X R, Zhu W J and Cheng Y 2005 *Phys. Rev. B* **72** 172502
[39] Haines J, Léger J M and Bocquillon G 2001 *Ann. Rev. Mater. Res.* **3** 1
[40] Ravindran P, Fast L, Korzhavyi P A, Johnnsson B, Wills J and Eriksson O 1998 *J. Appl. Phys.* **84** 4891
[41] Maachou A, Aboura H, Amrani B, Khenata R, Omran S B and Varshney D 2011 *Comp. Mater. Sci.* **50** 3123
[42] Chung D H and Buessem W R 1967 *J. Appl. Phys.* **38** 2010
[43] Ren D H and Cheng X L 2012 *Chin. Phys. B* **21** 127103
[44] Tsuchiya T and Kawamura K 2001 *J. Chem. Phys.* **114** 10086
[45] Maradudin A A, Montroll E W, Weiss G H and Ipatova I P 1971 *Theory of Lattice Dynamics in the Harmonic Approximation* (New York: Academic Press)
[46] Blanco M A, Pendás A M, Francisco E, Recio J M and Franco R 1996 *J. Mol. Struct.* **368** 245
[47] Flórez M, Recio J M, Francisco E, Blanco M A and Pendás A M 2002 *Phys. Rev. B* **66** 144112
[48] Francisco E, Recio J M, Blanco M A, Pendás A M and Costales A 1998 *J. Phys. Chem.* **102** 1595
[49] Francisco E, Blanco M A and Sanjurjo G 2001 *Phys. Rev. B* **63** 094107
[50] Poirier J P 2000 *Introduction to the Physics of the Earth's Interior* (Oxford: Cambridge University Press) p. 11
[51] Wentzcovitch R M, Chang K J and Cohen M L 1986 *Phys. Rev. B* **34** 1071
[52] Babu K E, Veeraiah A, Swamy D T and Veeraiah V 2012 *Chin. Phys. Lett.* **29** 117102
[53] Chang J, Chen X R, Zhang W and Zhu J 2008 *Chin. Phys. B* **17** 1377
[54] Liu L, Wei J J, An X Y, Wang X M, Liu H N and Wu W D 2011 *Chin. Phys. B* **20** 106201
[55] Liu X K and Tang B 2013 *Chin. Phys. Lett.* **30** 066201
[56] Debye P 1912 *Ann. Phys.* **39** 789
[57] Petit A T and Dulong P L 1819 *Ann. Chim. Phys.* **10** 395